Arabidopsis SPIRAL2 promotes uninterrupted microtubule growth by suppressing the pause state of microtubule dynamics

Maki Yao[1], Yoshinori Wakamatsu[1], Tomohiko J. Itoh[2], Tsubasa Shoji[1] and Takashi Hashimoto[1,*]

[1]Graduate School of Biological Sciences, Nara Institute of Science and Technology, Nara 630-0192, Japan
[2]Graduate School of Science, Nagoya University, Nagoya 464-8602, Japan
*Author for correspondence (e-mail: hasimoto@bs.naist.jp)

Accepted 22 April 2008
Journal of Cell Science 121, 2372-2381 Published by The Company of Biologists 2008
doi:10.1242/jcs.030221

Summary

SPIRAL2 (SPR2) of *Arabidopsis thaliana* is a microtubule-associated protein containing multiple HEAT repeats that are found only in the plant lineage. We show that SPR2 and SP2L, their closest *Arabidopsis* homolog, are expressed in various tissues with partially overlapping patterns, and *spr2-sp2l* double mutants exhibit enhanced right-handed helical growth. Fusion to green fluorescent protein (GFP) expressed under the control of the native regulatory elements showed that both SPR2 and SP2L were localized to cortical microtubules, mainly in particles of various sizes. Along the microtubule, the GFP- fused forms also distributed partly at the plus ends. In the *spr2*-mutant background, cortical microtubules were less dynamic, and the pause state – in which microtubules undergo neither growth nor shrinkage – increased at the plus ends. The continuous plus-end tracking of GFP-EB1 was occasionally interrupted in the mutant cells. Recombinant SPR2 protein promoted microtubule polymerization, and bound to microtubules with an N-terminal segment that contained two HEAT repeats as well as to those with a C-terminal region. In vitro analyses of microtubule dynamics revealed that SPR2 and SP2L suppressed the pause state at microtubule ends, thereby leading to enhanced microtubule growth. We propose that the SPR2-family proteins act on the pause state to facilitate a transition to microtubule growth.

Supplementary material available online at
http://jcs.biologists.org/cgi/content/full/121/14/2372/DC1

Key words: *Arabidopsis thaliana*, HEAT repeats, MAP, Microtubule, Pause, SPIRAL2

Introduction

Microtubules display dynamic instability in vitro and in vivo. Individual microtubules undergo polymerization and depolymerization with sporadic changes between the two states (Desai and Mitchison, 1997). In addition, microtubules without significant growth or shrinkage at their ends are often observed in cells and in certain experimental conditions in vitro, and are categorized as being in a third metastable state, i.e. pausing (Tran et al., 1997; Arnal et al., 2000). Polymerization dynamics of microtubules have been shown to be important for many cellular functions, such as cell division, polarization, motility and intracellular transport. In plant cells, microtubule dynamics are altered in tubulin mutants with twisting growth phenotypes, and have been implicated in the helical organization of cortical microtubule arrays and, consequently, changing of growth direction (Ishida et al., 2007).

Microtubule dynamics are intricately regulated by a variety of cellular factors that stabilize or destabilize the microtubule lattice. Many regulations of microtubule dynamics have been identified over the years; some regulator families are well conserved in yeasts, animals and plants, but others are specifically lost or gained in the plant lineage (Gardiner and Marc, 2003). A particularly interesting group of microtubule regulators, called microtubule plus-end-binding proteins (+TIPs), are specifically targeted or partially enriched at the microtubule plus end. The end binding 1 (EB1) family shows robust plus-end-tracking activity in vivo, and accumulates selectively at the growing microtubule ends without other proteins in vitro, as demonstrated for the yeast EB1 homologue Mal3 (Bieling et al., 2007). Other +TIPs include the CLASP and XMAP215 families that are characterized by the presence of several N-terminal TOG domains (Akhmanova and Steinmetz, 2008). One TOG domain contains six HEAT repeats, each comprised of a pair of parallel helices (Al-Bassam et al., 2007). A single TOG domain from yeast XMAP215 homologue Stu2p is capable of binding α-tubulin–β-tubulin heterodimers (Al-Bassam et al., 2007), whereas XMAP215 with five TOG domains binds the tubulin dimer in a 1:1 complex (Brouhard et al., 2008). The +TIP family members EB1, CLASP, and XMAP215 are evolutionally conserved in plants (Bisgrove et al., 2004). An example of plant-specific +TIPs is SPIRAL1, which accumulates at the growing microtubule end in some cell types of *Arabidopsis* plants (Nakajima et al., 2004; Sedbrook et al., 2004). Cellular and biochemical functions of these plant +TIPs, however, are poorly understood.

SPIRAL2 (SPR2) of *Arabidopsis thaliana* is a plant-specific microtubule-associated protein (MAP) containing multiple HEAT repeats clustered mostly at the N-terminus (Buschmann et al., 2004; Shoji et al., 2004). *SPR2* is allelic to *TORTIFOLIA1* (Furutani et al., 2000) and, hereafter, we refer to this locus as *SPR2*. Mutations in its gene result in right-handed helical growth in elongating aerial organs, such as the hypocotyl, petiole and petal (Furutani et al., 2000), and moderately affect the organization of cortical microtubule arrays in hypocotyl epidermal cells (Buschmann et al., 2004).

Recombinant SPR2 protein binds taxol-stabilized microtubules in vitro, whereas SPR2 overexpressed in *Arabidopsis* plants and in cultured tobacco cells decorates cortical microtubules, as well as other microtubule structures during the cell cycle (Buschmann et al., 2004; Shoji et al., 2004). In this study, we show that SPR2 is partially enriched at the microtubule plus end in vivo, reduces microtubule pausing and facilitates continued growth of cortical microtubules. Our biochemical and genetic studies also suggest that its closest *Arabidopsis* homologue, SP2L, possesses similar functions in the regulation of microtubule dynamics.

Results

SPR2 and *SP2L* are expressed in overlapping patterns

The *Arabidopsis* genome possesses one close homolog of SPR2, referred to here as SPIRAL2-Like (At1g50890; SP2L). SPR2 and SP2L both contain an N-terminal Ser/Thr-rich region and nine recognizable HEAT-repeat motifs, and exhibit overall amino acid identity of 48% to each other (Buschmann et al., 2004; Shoji et al., 2004). To compare the levels and patterns of *SPR2* and *SP2L* gene expression, we first conducted an reverse transcriptase (RT)-PCR-based analysis using a common primer set. The PCR primers hybridize to the sequences strictly conserved in the coding regions of these genes, and amplify a 987-bp *SPR2* cDNA fragment and an 879-bp *SP2L* cDNA fragment that can be distinguished from the amplification products from the genomic regions (Fig. 1A). Thus, the expression levels of *SPR2* and *SP2L* were directly compared after separation of the respective cDNA fragments on agarose gels. *SPR2* and *SP2L* were expressed in all the tissues examined, with the strongest expression in the inflorescence (Fig. 1B). In all tissues, *SPR2* was expressed more strongly than *SP2L*.

To explore the tissue- and cell-type expression patterns further, tandem copies of GFP were inserted at the 3′ end of the coding sequences of the *SPR2* and *SP2L* genomic DNA regions, and were expressed in transgenic *Arabidopsis* plants under control of their native *cis*-regulatory sequences. When several independent transgenic lines were examined (n=3 for SPR2-GFP and n=11 for SP2L-GFP), much stronger GFP fluorescence was observed in SPR2-GFP-expressing plants than in SP2L-GFP-expressing plants (Fig. 1C). SPR2-GFP signals were detected in all tissue types examined, but were considerably stronger in the root tips and the shoot meristem. SP2L-GFP was expressed at low levels in various cell types, whereas intense expression was seen at the hydathodes in cotyledons and relatively strong signals were detected in root hairs.

The Genevestigator organ-specific expression-profile database (Zimmermann et al., 2004) indicates that *SPR2* transcripts are present at relatively high levels in all organs, whereas the levels of SP2L transcripts are generally low but considerably abundant in root hair cells and pollen. These microarray-based expression profiles are thus consistent with our RT-PCR and promoter-expression-based analyses, and we conclude that *SPR2* and *SP2L* are expressed in almost all plant tissues in generally overlapping patterns, and that SPR2 expression is stronger than *SP2L* expression.

SPR2 and *SP2L* have redundant functions

To reveal possible functional redundancy, we examined phenotypes of transferred (T)-DNA insertion alleles of *SP2L* and their double mutants in combination with *spr2*. We identified three *sp2l*-mutant alleles in the ABRC T-DNA insertion pools, among which *sp2l-1* and *sp2l-3* did not express full-length *SP2L* transcripts (Fig. 2A). The two *sp2l* mutants were indistinguishable from the wild type in growth

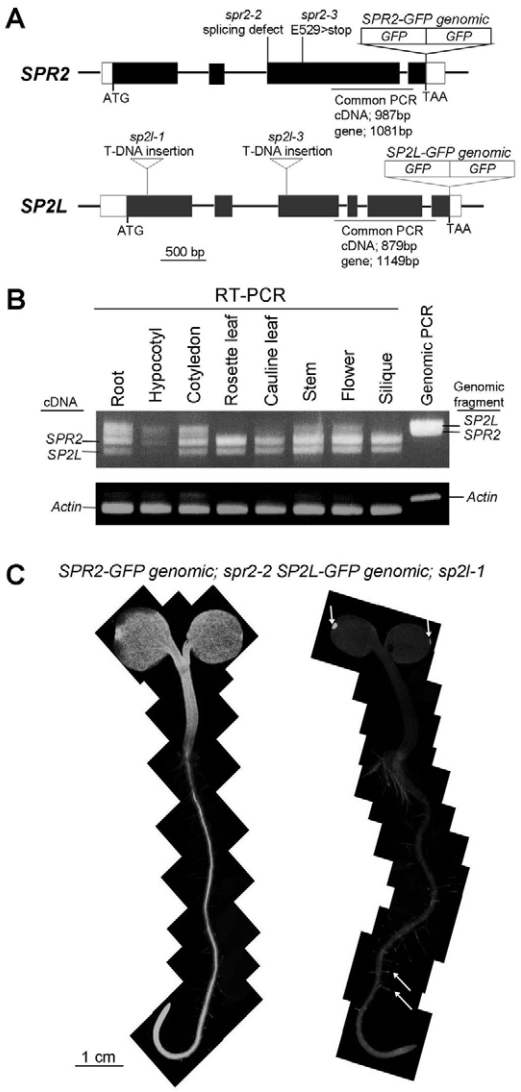

Fig. 1. Expression analysis of *SPR2* and *SP2L* genes. (A) Structure of *Arabidopsis SPR2* and *SP2L* genes. *SPR2* and *SP2L* consist of four and six exons (shown in thick bars), respectively. The protein-coding regions are in black, whereas the 5′- and 3′-untranslated regions are in white. Tandem copies of GFP were inserted just before the stop codons. PCR amplification results in products with different sizes that arise from cDNAs or genomic regions of *SPR2* and *SP2L*. Mutations in *spr2* and *sp2l* alleles are indicated. (B) Organ-specific expression patterns of *SPR2* and *SP2L*. Various organs of wild-type plants (Col ecotype) were analyzed for expression of *SPR2* and *SP2L* by RT-PCR, using a common primer set. *Actin8* was used as a control. The positions of cDNA fragments and genomic fragments are indicated on the left and right sides, respectively. (C) Tissue-specific expression patterns of *SPR2* and *SP2L*. GFP was expressed in the genomic context of SPR2 and SP2L, as indicated in (A). Four-day-old transgenic seedlings were observed by laser scanning confocal microscopy in the same low-power fields and at the equivalent gain levels. Arrows indicate hydathodes and root hairs.

and morphology. These two *sp2l* alleles were then crossed to two *spr2* alleles in the same ecotype (Shoji et al., 2004). Right-handed twisting of petioles in *spr2* was highly enhanced in the double mutants; the petioles of *spr2-2* and *spr2-3* rotated around the petiole axis roughly 180 degrees (upside down) and 90 degrees, respectively, whereas the petioles of the double mutant between *spr2-2* and *spr2l-1* (hereafter referred to as *spr2-2sp2l-1*) and *spr2-3sp2l-3* skewed further to 360 degrees and 180 degrees (Fig. 2B,C). Inflorescence of

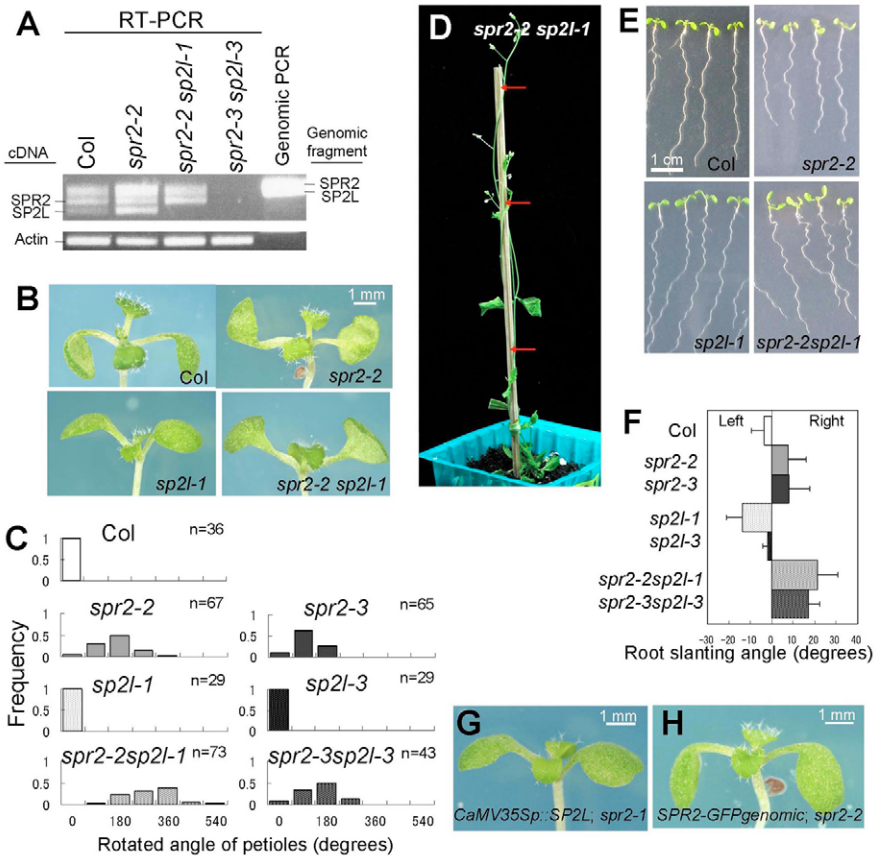

Fig. 2. Twisted growth of *spr2* is enhanced in *spr2sp2l*. (A) RT-PCR analysis of *SPR2* and *SP2L* expression in *spr2* and *spr2sp2l* mutant alleles. See Fig. 1A,B for experimental conditions. (B) Twisted petioles in 9-day-old seedlings of *spr2* and *spr2sp2l*. (C) Rotated angles of primary leaves in 2-week-old seedlings. The number of leaves analyzed is shown in the upper right corner. (D) Inflorescence stem of *spr2-2sp2l-1* climbs up a support, forming a right-handed helix. Three complete turns are shown by red arrows. (E) Root growth of 7-day-old seedlings grown on vertically placed hard agar plates. (F) Quantitative analysis of the root slanting angles. Roots that grew toward the right side of the plates were assigned the plus sign, whereas roots that grew to the opposite direction had the minus sign in the root-slanting angles. Error bars represent standard deviations of the means. (G) Overexpression of SP2L under the control of the CaMV35S promoter rescued the twisting phenotype of *spr2-1*. (H) SPR2-GFP expressed in the genomic context rescued the twisting phenotype of *spr2-2*. Nine-day-old seedlings are shown in G and H.

the double mutants twined up a support in a right-handed helix, a phenotype not observed in either single mutants (Fig. 2D). The *spr2sp2l* double mutant roots grew slightly towards the right side of the agar plates (as viewed from above; see Fig. 2E,F). Although *SPR2* and *SP2L* are expressed in root hairs; we observed no root hair phenotype in single and double mutants. These phenotypic analyses of single and double mutants indicate that mutations in *SP2L* enhance the right-handed twisting phenotype of *spr2*.

When *SP2L* was expressed under the control of the CaMV 35S promoter in *spr2*, the resulting transgenic plants grew like wild-type plants without a skewing phenotype in the leaf petiole and in the root (Fig. 2G). Therefore, SP2L can complement the loss of SPR2 function when expressed strongly. In summary, SPR2 and SP2L have similar and overlapping functions in the regulation of anisotropic growth.

SPR2-GFP is partly localized at the plus end of microtubules in vivo

Previous studies have shown that the SPR2-GFP fusion protein labeled microtubules in the cortical array, preprophase band, metaphase spindle and phragmoplast when stably overexpressed under the control of the CaMV 35S promoter in transgenic *Arabidopsis* plants and tobacco BY-2 cells (Buschmann et al., 2004; Shoji et al., 2004). In this study, native cis-regulatory sequences were used to express SPR2-GFP and SP2L-GFP so that the precise subcellular localization of SPR2 and SP2L at the endogenous expression level may be revealed. Expression of SPR2-GFP in its genomic context complemented the *spr2* mutant (Fig. 2H), whereas SP2L-GFP expressed in its genomic region ameliorated the twisting phenotype of *spr2sp2l* to the level of the *spr2*-single mutant (data not shown). These results indicate that SPR2-GFP and SP2L-GFP are functional.

Both SPR2-GFP and SP2L-GFP labeled cortical microtubule array in all the cells where the transgenes were expressed. In many cell types, the GFP fluorescence was observed in punctate patterns of various sizes that aligned on the microtubule lattice (Fig. 3A). These distinct GFP particles appeared to be aggregates or oligomers of SPR2-SP2L–GFP. The intersections of two crossing microtubules are often labeled more intensely than neighboring regions (Fig. 3B). In hypocotyl epidermal cells, we observed events in which SPR2-GFP particles were ‘picked up’ by the shrinking microtubule end, causing an increase in GFP signal at the microtubule end as the shrinkage continued (Fig. 3C and supplementary material Movie 1). When one motile particle encountered another on the same microtubule, they yielded an enhanced GFP signal (Fig. 3D and supplementary material Movie 2). Also, one particle did sometimes divide into two smaller ones. Such merging and fission of the SPR2-SP2L–GFP particles may explain the observed variation in size.

The GFP-fused proteins also faintly labeled the entire length of microtubules, indicating that SPR2-SP2L–GFP proteins have weak affinity for the microtubule lattice. A concentration of the SPR2-SP2L–GFP signals was sometimes observed at the plus ends of microtubules (Fig. 3E and supplementary material Movie 3). Interestingly, the GFP signals appeared to be concentrated not only on the growing end but also on the shrinking end. Guard cells of SPR2-GFP plants contained few large fluorescent foci but had cortical arrays decorated along their length with the fusion protein (Fig. 3F). There, SPR2-GFP accumulated at the plus end of microtubules that grew outward from the inner face of the guard cells (Fig. 3G and supplementary material Movie 4), although the

accumulation of SPR2-GFP at the growing plus end was not as extensive as that of GFP-EB1 (supplementary material Fig. S1), indicating that SPR2 has weaker affinity for the microtubule ends than EB1.

Polymerizing microtubule ends are occasionally stalled in *spr2* cells

It has been shown that the distribution of cortical microtubules was biased toward left-handed arrays in hypocotyl epidermal cells with *tortifolia*, an allele of *spr2*, compared with wild-type microtubules (Buschmann et al., 2004). To test whether alterations of microtubule dynamics underlie the observed shift in distribution, we monitored cortical microtubules beneath the outer epidermal walls of hypocotyls and petioles by using GFP-tagged β-tubulin (GFP-TUB6). The rather mild defect in the organization of *tortifolia* microtubules prompted us to compare the microtubule status in four samples; wild type, *spr2-2* and *spr2-2sp2l-1* double mutants, and a transgenic plant line in which overexpressed SPR2 complemented the *spr2-2* phenotype (SPR2ox;*spr2*) (Fig. 4). In both 4-day-old and 7-day-old wild-type hypocotyls, microtubule orientations were distributed over a broad range from transverse to oblique angles. We did not observe a bimodal distribution consisting of two distinct populations of left- and right-handed arrays in the 7-day-old wild-type hypocotyls, as reported by Buschmann et al. (Buschmann et al., 2004). Rotary movements of cortical microtubule arrays reported in *Arabidopsis* hypocotyl epidermal cells (Chan et al., 2007) might underlie this discrepancy. In *spr2* hypocotyls, microtubule orientations were still distributed broadly, but the average angles of microtubule arrays were shifted toward left-handed orientations. Analysis of the SPR2ox;*spr2* line revealed that overexpression of SPR2 complemented this moderate defect in microtubule orientations of *spr2*. Moreover, the *spr2sp2l* double mutant showed

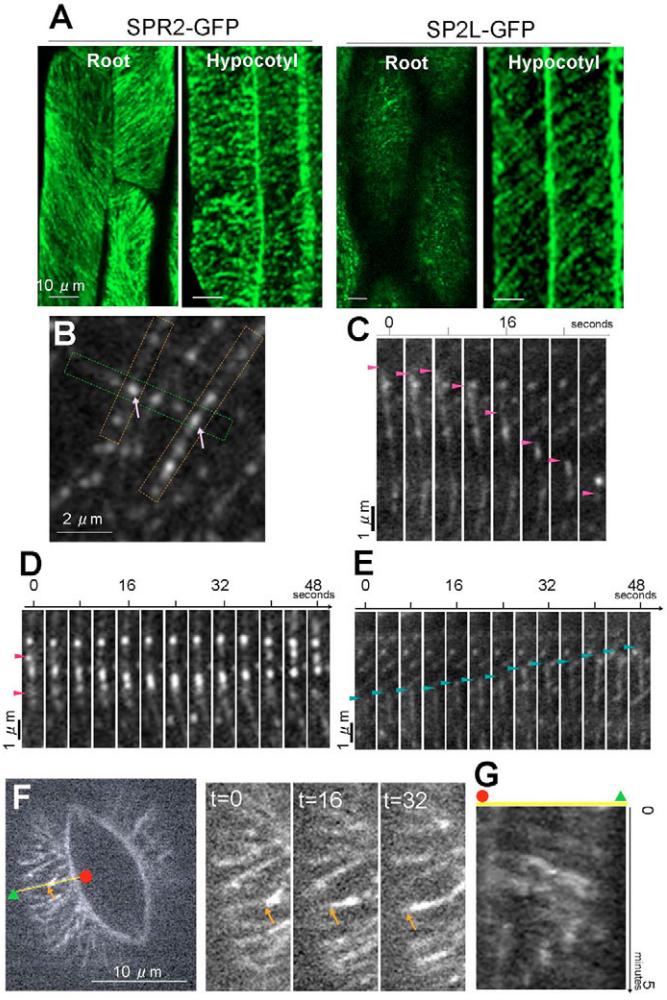

Fig. 3. Intercellular localization of SPR2-GFP and SP2L-GFP proteins. (A) SPR2-GFP and SP2L-GFP are expressed under the control of native regulatory elements in *spr2-2* and *sp2l-1*, respectively. Seven-day-old seedlings were analyzed with laser scanning confocal microscopy. (B) SPR2-GFP particles are found at intersections (arrows) of crossing microtubules (marked by dotted lines) in hypocotyl epidermal cells. (C) SPR2-GFP associated with a shrinking microtubule end (arrowheads). (D) SPR2-GFP particles (arrowheads) moved along the microtubule lattice, collided and then merged. (E) SPR2-GFP is abundant at the polymerizing plus end (arrowheads). (F) SPR2-GFP labels cortical microtubules in cotyledon guard cells of 4-day-old seedlings. Three successive micrographs every 16 seconds are shown. The accumulation of SPR2-GFP at the growing microtubule tip is indicated by arrows. (G) Kymograph of SPR2-GFP movement on the yellow line shown in (F).

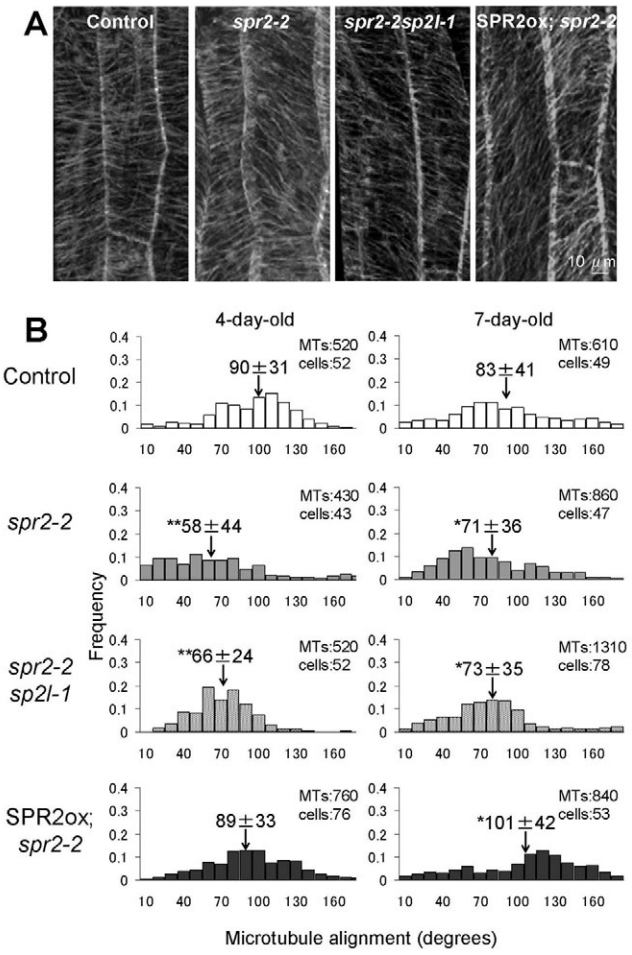

Fig. 4. Microtubule distribution in seedling hypocotyls. Cortical microtubules were visualized by GFP-TUB6 in the upper and lower regions of epidermal cells in 4-day-old and 7-day-old seedlings, respectively. (A) Images from 4-day-old seedlings. (B) Distribution of microtubule orientations. Transverse microtubule orientation is set at 90 degree, whereas orientations in left-handed helical arrays have values less than 90 degrees. The average microtubule angles are indicated with arrows above histograms. Asterisks show statistically significant differences from control (*t*-test; $*P<0.05$, $**P<0.01$).

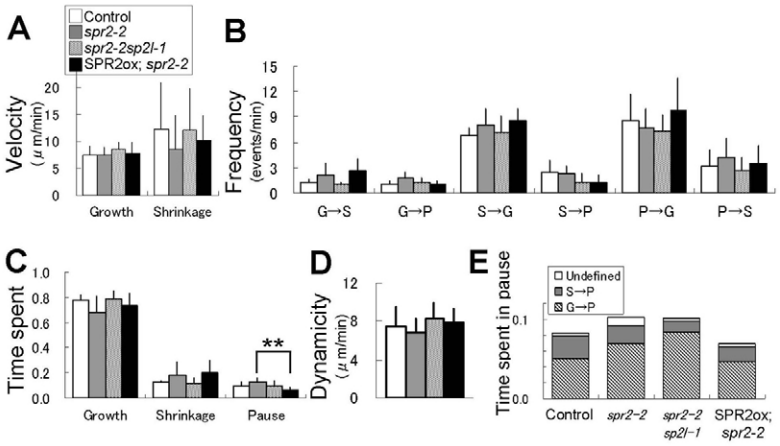

Fig. 5. Parameters of microtubule dynamics in planta. Microtubule dynamic behavior of the plus end was measured in the GFP-TUB6 background. (A) Growth and shrinkage velocities. (B) Transition frequencies among growth (G), shrinkage (S) and pause (P). (C) Total time spent in growth, shrinkage, and pause. Data shown are means ± s.d. Statistical significance (*t*-test; ***P*<0.005) is obtained between *spr2* and the SPR2-overexpressing line. (D) Microtubule dynamicity – a measure of the total tubulin exchange at microtubule plus ends. (E) Time spent in the pause state was classified, depending on the previous history of the microtubule ends. When the microtubules were in the pause state at the start of observation, they were categorized as 'undefined'. Sample values were: control, *n*=23 microtubules and *t*=38.6 minutes; *spr2-2*, *n*=32 microtubules and *t*=58.8 minutes; *spr2-2sp2l-1*, *n*=22 microtubules and *t*=50.7 minutes; SPR2ox;*spr2-2*, *n*=22 microtubules and *t*=36.8 minutes.

a considerably sharper distribution of microtubule orientations, which were biased toward left-handed arrays. Similar analyses of microtubule orientations in the epidermal cells of 7-day-old petioles (supplementary material Fig. S2) further confirmed our observation that the lack of SPR2/SP2L biases microtubule orientations toward left-handed arrays.

We next monitored the dynamic plus end of cortical microtubules in the epidermal cells of hypocotyls, and calculated the velocities of growth and shrinkage, frequencies of phase transition between growth, shrinkage, and pause, and the total time spent in these three phases (Fig. 5). Since plant microtubules exhibit dynamic behavior far more often than animal microtubules (e.g. Shaw et al., 2003), pauses in our in vivo studies were defined as a state during which a growth rate of less than 1 μm/minute continued for more than 4 seconds. This minimum period in the pause definition is shorter than the values generally used for animal studies [e.g. 30 seconds in Brittle and Ohkura (Brittle and Ohkura, 2005)], and thus our pauses include mini-pauses. Most of the dynamics parameters of wild type, *spr2*, *spr2sp2l* and SPR2ox;*spr2* were not remarkably different. Microtubule dynamicity, a composite measurement of all the tubulin dimers gained or lost per unit time (Toso et al., 1993), was statistically indistinguishable among the four samples as well. However, statistically significant difference (Student's *t*-test; $P<0.005$) was observed between *spr2* (0.131±0.032; mean ± s.d.) and SPR2ox;*spr2* (0.068±0.019) in the time spent in the pause state (Fig. 5C,E). The plus end of microtubules in *spr2* cells spent considerably more time in the stationary pausing state than did that of SPR2ox;*spr2* cells, whereas the wild-type and s*pr2sp2l* values were in between the two. To categorize the paused state more precisely, we took into account the previous history of microtubules to see whether a growing or shrinking microtubule resulted in the pause. This analysis revealed that, during the growth phase, microtubules of *spr2* and *spr2sp2l* tend to be halted in pauses, compared with growing microtubules of wild-type and SPR2ox;*spr2*.

To further evaluate the plus-end state of microtubules in planta, we monitored the dynamics of GFP-EB1, which continuously tracked the plus end of polymerizing microtubules as comets (Fig. 6). In epidermal cells of wild-type hypocotyls, the trajectory of GFP-EB1 generally followed a largely straight path. Occasionally, a growing microtubule changed its path abruptly to a new direction at a shallow angle (mostly <15 degrees; arrows in Fig. 6A), probably reflecting a collision event with another microtubule and subsequent incorporation into a microtubule bundle (Dixit and Cyr, 2004). The kymographs of such curved trajectories of GFP-EB1 showed uninterrupted linear tracks without gaps, indicating that growing microtubules were not stalled by the microtubule-microtubule collision events. In contrast, GFP-EB1 comets in *spr2* cells frequently deviated from a linear trajectory (supplementary material Table S1), and the abrupt curving events occurred multiple times (up to five times) during the life of a single microtubule (Fig. 6B and supplementary material Movie 5). Another notable feature of GFP-EB1 dynamics in *spr2* cells was that the EB1-labeled microtubule ends frequently stalled for several seconds, and then started to track a new growth path again at the previous velocity. This irregular movement of GFP-EB1 in the absence of SPR2 was typically shown in the kymographs where the linear trajectory of GFP-EB1 was interrupted by vertical gaps of several seconds. GFP-EB1 was partly retained at the stalled plus end, especially at the beginning of the pause. Not only did the frequency of pauses increase but longer pauses of 8 seconds or more were almost only observed in *spr2* cells (supplementary material Table S2). Some of the abrupt changes in the GFP-EB1 trajectory occurred during the paused state, but other turns happened during continuous growth, as seen in wild-type cells. When the growth velocity of the plus end was measured with the aid of GFP-EB1 in epidermal cells of hypocotyl and petiole, the distribution in *spr2* cells was slightly shifted toward slower growth rates, as seen in the greater proportion of slowly growing microtubules compared with the wild-type distribution (Fig. 6C). Notably, the plus end in *spr2* cells spent about 6% (5.5% in hypocotyl cells and 5.8% in petiole cells) of the growth phase in the paused state; in wild-type cells, the paused state accounted for less than 1% of the total life of plus ends. We conclude that SPR2 secures uninterrupted growth at the plus end of cortical microtubules in plant cells.

Recombinant SPR and SP2L proteins promote dynamicity of microtubule ends

Altered microtubule behavior in the *spr2* mutant suggests that SPR2 protein modulate microtubule functions directly. To test this possibility, we analyzed the effects of recombinant SPR2 and SP2L proteins on the microtubule dynamics in vitro. SP2L was included in the in vitro assay because it has a redundant and similar function to SPR2 as shown above, and because recombinant SP2L bound to taxol-stabilized microtubules in vitro (supplementary material Fig. S3). SPR2 and SP2L were produced in *E. coli* as proteins fused to the trigger factor (TF), which enhanced the solubility of the recombinant proteins, and purified to apparent homogeneity.

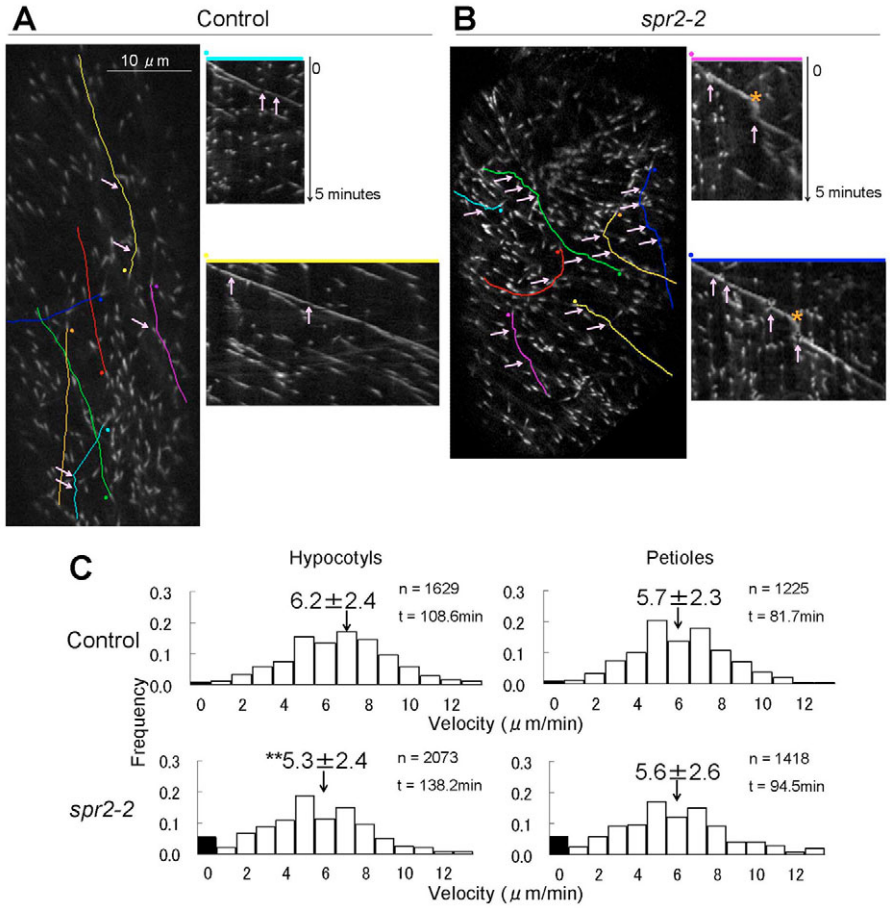

Fig. 6. Microtubule plus-end tracking with GFP-EB1. (A,B) Tracks of several GFP-EB1b comets were followed for 5 minutes in hypocotyl epidermal cells of control (A) and *spr2-2* (B) plants, and are indicated by colored lines. Circles at one end of GFP-EB1 trajectories show the start points of measurements, whereas arrows indicate abrupt changes in the trajectory. Kymographs are shown for two representative trajectories, in which transient stops of GFP-EB1 are indicated by asterisks. (C) Histograms of GFP-EB1 velocity distribution in hypocotyls and petioles of control and *spr2-2* plants. Stationary GFP-EB1 comets with a velocity less than 1 μm/minute are shown in black bars. The stationary comets were excluded when the mean values (± s.d.) of the velocity were calculated. Velocity distributions of *spr2* cells and control cells were significantly different (*t*-test; $^{**}P<0.01$).

Dynamics of microtubules was analyzed by using dark-field microscopy, and parameters of microtubule dynamics were quantified for both plus and minus ends. In our in vitro assay, we set the incubation temperature at 27°C, instead of the usually used 30°C. At this lower temperature, dynamic instability was moderately reduced so that otherwise infrequent pauses could be observed more readily. In this in vitro assay, a microtubule growth state during which a growth rate of less than 0.15 μm/minute continued for more than 30 seconds was counted as a pause.

When supplied at 0.2 μM or 0.4 μM, TF-SPR2 and TF-SP2L did not considerably affect velocities of growth and shrinkage of the plus end (Fig. 7B), whereas transition frequencies from growth to pause and from shrinkage to pause tended to be suppressed (Fig. 7C). These changes in dynamicity manifest in a decreased total period spent in pauses and an increased time spent in the growth phase (Fig. 7D). The reduced pausing time contributed to a moderate increase in dynamicity at the plus end (Fig. 7E). Statistical significance, however, was assigned only to a few parameters, due to high intrinsic variability among the dynamics of individual microtubules. At the minus end, TF-SRR2 and TF-SP2L also showed a tendency to suppress pauses and to increase the time spent in growth, although the values of dynamics were not so affected (supplementary material Fig. S4). Overall, recombinant SPR2 and SP2L proteins (in their TF-fused forms) promoted microtubule dynamicity by suppressing the paused state and prolonging the growth duration.

We confirmed the polymerization-promoting activity of SPR2 by using a turbidity assay (Fig. 7F). TF-SPR2 at 0.5 μM significantly promoted the formation of microtubule polymers from the 17.5 μM tubulin solution at 37°C, compared with the TF control at the same concentration.

SPR2 possesses at least two microtubule-binding regions

Both SPR2 and SP2L contain an N-terminal Ser/Thr-rich region and nine predictable HEAT-repeat motifs which are clustered in the N-terminal half of the protein. To identify microtubule-binding region(s), we expressed various SPR2 fragments fused to thioredoxine and polyhistidine in E. coli, and purified them to near homogeneity. The N-terminal region containing the Ser/Thr-rich region and the first seven HEAT motifs ($SPR2^{1-331}$) and the C-terminal region containing the eighth and ninth HEAT motifs ($SPR2^{498-864}$) bound taxol-stabilized microtubules almost as efficiently as the full-length SPR2, but the middle region ($SPR2^{327-499}$) did not (Fig. 8). The fusion of these fragments to glutathione S-transferase (GST) gave the same results, although microtubule-binding GST-SPR2 showed considerable microtubule-bundling activity, probably due to the artificial dimerization caused by GST (supplementary material Fig. S5). On testing smaller fragments of the N-terminal SPR2 region, we narrowed down the moderate microtubule-binding activity to a fragment only consisting of the fourth and fifth HEAT motifs ($SPR2^{163-248}$). These results indicate that SPR2 contains at least two distinct microtubule-binding regions and that a tandem repeat of two SPR2-HEAT motifs possesses significant affinity for microtubule polymers.

When the N-terminal, middle and C-terminal regions ($SPR2^{1-331}$, $SPR2^{327-502}$ and $SPR2^{498-864}$, respectively) were fused to the N-terminus of GFP and expressed stably under the control of the CaMV

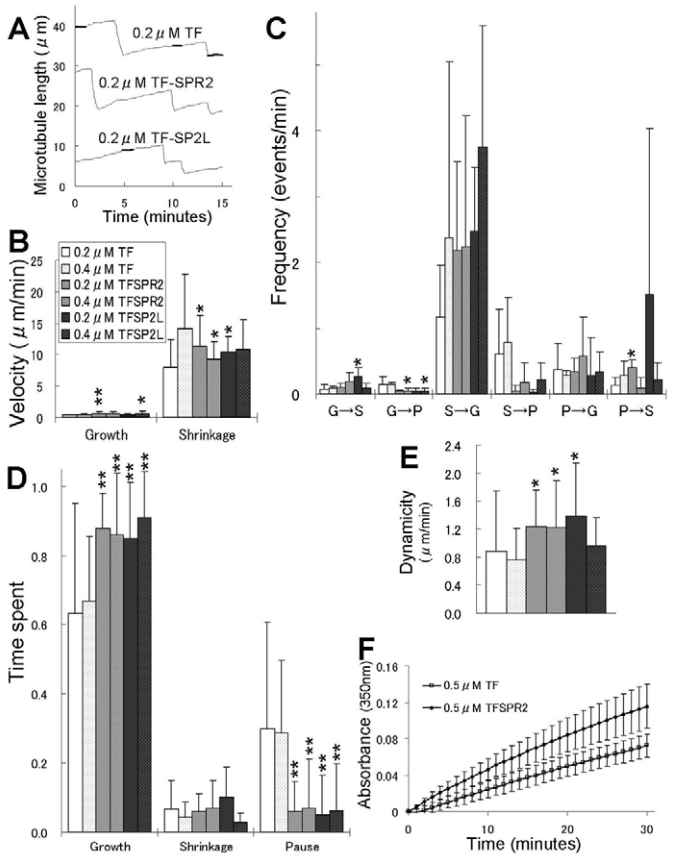

Fig. 7. Parameters of microtubule dynamics in vitro. Dynamic behavior at the plus end of in vitro assembling microtubules was measured at 27°C in the presence of Trigger Factor (TF), TF-SPR2, or TF-SP2L at concentrations of 0.2 μM and 0.4 μM, by using dark field microscopy. (A) Dynamic instability profiles of microtubules at the plus end in the presence of 0.2 μM SPR2 or 0.2 μM SP2L. The pause state is indicated by thick lines. (B) Growth and shrinkage velocities. (C) Transition frequencies among growth (G), shrinkage (S) and pause (P). (D) Total time spent in growth, shrinkage, and pause. (E) Microtubule dynamicity. Data shown are means ± s.d. Statistical significance (*t*-test; **P*<0.05 and ***P*<0.01) is shown for TF-SPR2 or TF-SP2L vs TF control at the same concentration. (F) TF-SPR2 increases microtubule polymerization. Turbidity of the 17.5 μM tubulin solution in the presence of 0.5 μM TF (white squares) or 0.5 μM TF-SPR2 (black circles) was monitored at 350 nm and at 37°C. The values are means (± s.d.) from four independent experiments. Sample values; 0.2 μM TF, *n*=16 microtubules and *t*=136.9 minutes; 0.4 μM TF, *n*=12 microtubules and *t*=130.9 minutes; 0.2 μM TF-SPR2, *n*=28 microtubules and *t*=333.1 minutes; 0.4 μM TF-SPR2, *n*=17 microtubules and *t*=204.5 minutes; 0.2 μM TF-SP2L, *n*=20 microtubules and *t*=245.4 minutes; 0.4 μM TF-SP2L, *n*=20 microtubules and *t*=249.8 minutes.

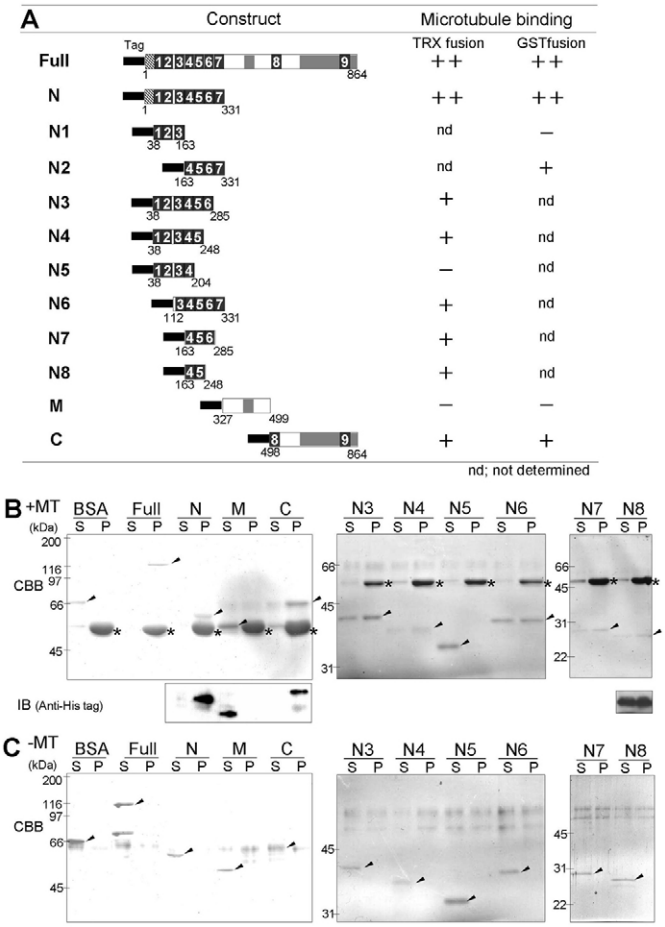

Fig. 8. Identification of microtubule binding regions in SPR2. (A) Diagram of SPR2 fragments used in the microtubule co-sedimentation assay. The N-terminal Ser/Thr-rich region is indicated by hatched boxes, while the regions conserved among SPR2, SP2L, and their orthologs in other plant species are shown by gray boxes. Predictable HEAT repeats are numbered from the N-terminus of SPR2. Recombinant proteins are fused to a thioredoxin (TRX)/poly-His tag or to GST, expressed in *E. coli*, and purified. When fusion proteins were recovered mostly in the pellet fraction after co-sedimentation with taxol-stabilized microtubules, the symbol ++ was given, while + indicates a roughly equal recovery in both supernatant and pellet fractions. The minus symbol shows no microtubule binding. (B) SDS-PAGE analysis of SPR2 fragments after co-sedimentation with taxol-stabilized microtubules. Microtubules and SPR2 fragments were mixed and centrifuged at 100,000 ***g***, and then supernatants (S) and pellets (P) were separated on SDS-PAGE gels. Staining with the Coomassie Brilliant Blue dye (CBB; upper images) detected tubulin (*), BSA and SPR2 fragments (arrowheads). In several samples, TRX-fused SPR2 fragments were also detected by immunobloting (IB) with an anti-polyHis antibody (lower images). (C) Sedimentation of the SPR2 fragments used in (B), in the absence of microtubules, and analysis as in (B). All the tested proteins were recovered in the soluble fraction in the absence of microtubules.

35S promoter in tobacco BY-2 cells, the fusion proteins did not label cortical microtubules (supplementary material Fig. S6). The same constructs did not complement the twisting phenotype of *spr2-2*, either (data not shown). These results suggest that efficient in vivo localization to cortical microtubules and microtubule-regulating function require a nearly full-length SPR2 protein.

Discussion

SPR2 and SP2L are functionally redundant MAPs

The main structural feature of SPR2 and SP2L is the HEAT repeats; nine repeats are predicted from structure prediction algorithms but there might be additional ones. The two distinct HEAT-repeat-containing fragments that are conserved in SPR2 and SP2L bind directly to microtubules in vitro. In planta, both MAPs colocalize with cortical microtubules; when expressed at endogenous levels under the control of genomic regulatory elements, GFP-fused forms of these MAPs decorate microtubules with a punctate pattern, as well as along the entire length of microtubules. Functionally, recombinant SPR2 and SP2L proteins expressed in *E. coli* affect the dynamics of microtubule ends in an indistinguishable manner. These conserved characteristics suggest that SPR2 and SP2L have very similar functions in regulating microtubule dynamics.

Although the two *sp2l* mutants with the T-DNA insertion in the *SP2L* coding region appeared to be null alleles, we did not observe any morphological abnormalities in these mutants, probably reflecting much lower expression levels of SP2L than of SPR2 in all tissues examined. The in vivo function of SP2L may be revealed by the fact that *sp2l* mutants showed abnormal skewing phenotypes when challenged with low doses of microtubule-depolymerizing drugs (data not shown), and that the twisting phenotypes and the microtubule defects of *spr2* were augmented in the *sp2l* background. Suppression of the *spr2* phenotypes by overexpression of SP2L further supports that SPR2 and SP2L are MAPs of the same functionality.

SPR2 promotes continued growth of microtubules by suppressing pauses

In vitro, the recombinant SPR2 and SP2L proteins significantly reduced the amount of time that microtubules spend pausing and rendered microtubule ends more dynamic. Under our experimental conditions, microtubule assembly was promoted by these MAPs. In plant cells, the effect of SPR2 was most clearly seen in the continuous growth of microtubule plus ends, as visualized with GFP-TUB6 and GFP-EB1. Our in planta observation suggests that SPR2 (and probably SP2L as well) suppresses pausing of polymerizing microtubules and thereby insures uninterrupted growth at the plus end. Occasional deviation of GFP-EB1-labeled plus ends from the previous trajectory in *spr2* cells might be caused if the pausing plus ends have a weakened association with the plasma membrane.

The proposed function of SPR2 and SP2L as suppressors of the pause state requires its localization at microtubule ends. A large proportion of the SPR2-GFP in *Arabidopsis* cells was found to be distributed in a punctate pattern along the length of cortical microtubules. The abundant SPR2 particles do not appear to represent microtubule ends, as judged from their generally stationary nature and occasional irregular motility. The localization of SPR2-GFP at tips, however, is evident in cortical microtubules of stomatal guard cells, and is sporadically seen in microtubules of epidermal cells. A weak association with the plus end of microtubules may be an intrinsic property of SPR2 because its overexpression does not enhance the localization at tips. Notably, SPR2-GFP appeared to be concentrated at both the growing and shrinking ends, which may provide a clue as to its tip-targeting mechanism. Double labeling of SPR2 and EB1 with different fluorescent proteins is necessary to follow the tracking of tips at a higher resolution.

Microtubule pausing for longer than 30 seconds has been frequently observed in animal cells (e.g. Rusan et al., 2001), but are rare in interphase plant cells (Shaw et al., 2003; Nakamura et al., 2004; Vos et al., 2004). When microtubules are assembled in vitro from tubulins purified from animal sources, they usually do not exhibit substantial pausing during phases of polymerization and depolymerization unless dynamic instability is reduced (Grego et al., 2001) (this study), indicating dynamic instability is suppressed or pausing is promoted by cellular factors in animal cells. Microtubules assembled in vitro from purified carrot tubulins are more dynamic than those of animals (Moore et al., 1997). The intrinsically more dynamic property of plant microtubules might contribute to rare incidences of pausing in plant cells. In addition, plant factors that suppress the pause state should promote high dynamic instability in interphase plant cells.

It has been proposed that the pause state is an obligate intermediate between polymerization and depolymerization, and microtubules can theoretically transform into either growth or shrinkage from this state (Tran et al., 1997). Recently, microtubule assembly dynamics were studied at the nanoscale by using optical tweezers to track microtubule polymerization against microfabricated barriers (Schek, III et al., 2007). The high-resolution study revealed that a pause at low resolution is composed of repeated switches between brief growth and shortening excursions, and suggests that individual protofilaments with GTP caps of varying lengths at the microtubule plus end undergo stochastic micro-growth and micro-shrinkage during a pause. Theoretically, +TIPs that recognize the pausing-end structure and promote polymerization or depolymerization of the protofilaments should suppress the pause state.

Although EB1, XMAP215, and other +TIPs are often discussed as sharing a common mechanism to regulate microtubule tips (Slep and Vale, 2007), recent studies show distinct mechanisms for tip tracking and altering microtubule dynamics. EB1 and its fission yeast homologue Mal3p apparently track tips by treadmilling (Tirnauer et al., 2002; Bieling et al., 2007), whereas XMAP215 is recruited to the tips by a diffusion-facilitated 'tip-tracking' mechanism (Brouhard et al., 2008). At the plus end, the individual XMAP215 proteins move with both assembling and disassembling microtubule tips. XMAP215 increases the growth rate of microtubules tenfold in vitro (Gard and Kirschner, 1987), whereas it depolymerizes microtubules in the absence of free tubulin (Brouhard et al., 2008). This reversibility suggests that XMAP215 is capable of promoting either assembly or disassembly by stabilizing a transient tubulin dimer when it collides with the microtubule end. The proposed function of XMAP215 might explain the anti-pausing activities observed under some experimental conditions. XMAP215 depolymerizes microtubules stabilized with GMPCPP, a slowly hydrolyzed analog of GTP, that are proposed to mimic the pausing state (Shirasu-Hiza et al., 2003). Depletion of Mini spindles, the *Drosophila* homologue of XMAP215, in cultured cells dramatically increases microtubule pausing at the cell periphery (Brittle and Ohkura, 2005). SPR2 bears several similar properties to XMAP215: the presence of multiple HEAT repeats, a plus-end localization and effects on the pausing state. Clarification of whether these similarities extend to the mechanisms modulating microtubule dynamics awaits further biochemical characterization of SPR2, preferably including a single-molecule microscopy assay.

SPR2 particles on the microtubule lattice

The cellular functions, if any, of SPR2 with the punctate distribution are not apparent. We observed that SPR2 molecules increase or decrease in size when they fuse or undergo fission, indicating that SPR2 molecules associate with each other with weak affinity. Recombinant SPR2 also tends to aggregate and precipitate in the buffer at low-salt concentrations (our unpublished results). The movement of SPR2 along the microtubule length might occur by capturing the disassembling microtubule tips, by one-dimensional diffusion on the lattice, or by the actions of motor proteins. These particles might serve as a reservoir of SPR2 molecules, loading SPR2 onto microtubule ends when polymerizing or depolymerizing microtubule ends pass through them. In this scenario, SPR2 is proposed to bind microtubules with higher affinity for the ends than the lattice, and self-associates to form flexible oligomers. Studies of the in vitro localization and dynamics of SPR2 on individual microtubules at a high resolution might provide further information.

It is worth noting that other *Arabidopsis* HEAT-repeat-containing MAPs, MOR1 (Twell et al., 2002; Kawamura et al., 2006) and AtCLASP (Ambrose et al., 2007; Kirik et al., 2007), have a punctate

distribution on cortical microtubules. The tobacco MOR1 homolog also labels cortical microtubules with a punctate pattern (Hamada et al., 2004). Animal and yeast orthologs of these MAPs are preferentially recruited to microtubule ends (Akhmanova and Steinmetz, 2008), although a punctate distribution along interphase microtubules has also been reported for *Drosophila* Msps (Brittle and Ohkura, 2005). *Arabidopsis* CLASP was shown to be partially enriched at the plus end of microtubules (Ambrose et al., 2007; Kirik et al., 2007), as seen in SPR2. MOR1 – a member of the XMAP215 family – is not particularly concentrated at tips at all stages of the cell cycle (Kawamura et al., 2006). The punctate distribution on cortical microtubules might be a common feature of potentially tip-targeting plant MAPs composed of HEAT repeats, and there may be an unrecognized mechanistic relationship between abundant MAP particles on the length of microtubules and their partial concentration at microtubule ends.

Materials and Methods

Plant materials and growth conditions

The *spr2-2* and *spr2-3* mutant alleles have been described (Shoji et al., 2004). A T-DNA insertion allele of *SP2L*, *sp2l-1*, was isolated from mutant pools at the *Arabidopsis* Knockout Facility of the University of Wisconsin Biotechnology Center, whereas *sp2l-3* (SALK_142747) was ordered from the SALK T-DNA insertion line collection. The SPR2 overexpression line in the *spr2-2* background was described previously (Shoji et al., 2004). GFP-TUB6 and GFP-EB1b microtubule-labeling lines were described previously (Nakamura et al., 2004; Abe and Hashimoto, 2005). Plants were grown as described previously (Furutani et al., 2000). Petiole rotation, root angle and root length were measured for seedlings grown on a nutrient medium solidified with 1.0% (w/v) agar.

Transgenic plants

The Isolation and manipulation of DNA were performed by using standard molecular techniques. After the SPR2 genomic region including a 2035-bp region 5′ upstream of the initiation ATG and a 964-bp region 3′-downstream of the stop codon was subcloned into pDONR221 by PCR and BP reactions, *Kpn*I and *Not*I sites were introduced in place of the stop codon by PCR. The SP2L genomic fragment prepared similarly contained a 2531-bp 5′-upstream region and a 1038-bp 3′-downstream region. A duplicated GFP fragment was excised as a *Kpn*I-*Not*I fragment from pBS-2xrsGFP (Crawford and Zambryski, 2000), and inserted into the C-termini of SPR2 and SP2L in the above vectors. The SPR2-SP2L–GFP genomic fragments were then transferred to a Gateway binary vector pGWB1 (Nakagawa et al., 2007) by the LB reaction. A full-length SP2L cDNA was cloned downstream of the CaMV 35S promoter in pBI121 (Clontech). These binary vectors were introduced into the *Agrobacterium tumefaciens* strain MP90 and then used to transform *Arabidopsis* plants (wild type and mutant alleles) by the floral dip method (Clough and Bent, 1998). Fluorescent images of SPR2-GFP and SP2L-GFP in transgenic plants were observed using a confocal laser-scanning microscopy (Nikon C1-ECLIPSE E600).

Production of recombinant proteins

The vector pTH-SPR2 has been described previously (Shoji et al., 2004). Full-length SPR2 and SP2L cDNAs were cloned into pColdTF (Takara) that had been digested with *Kpn*I-*Sal*I and *Kpn*I-*Bam*HI, respectively. SPR2 cDNA fragments were cloned into *Kpn*I-*Sal*I-digested pET32b (Novagen). Recombinant proteins were produced in the *E. coli* strain BL21 DE3 or Rosetta DE3 (Novagen). Proteins were extracted by sonication and affinity-purified by using Ni-Sepharose resin (GE Healthcare) or Ni-NTA resin (Qiagen), according to the manufacturers' instructions. The eluted proteins were further purified by anion-exchange chromatography using Q-Sepharose fast-flow resin (GE Healthcare). The buffer of the purified recombinant proteins was changed to the PEM buffer (0.1 M PIPES pH 7.0, 1 mM EGTA, 1 mM $MgCl_2$, 1 mM DTT and 1 mM PMSF) by passing through the PD-10 column (GE Healthcare).

Reverse transcriptase PCR analysis

RNA was extracted using the RNeasy Plant Mini kit (Qiagen), and first-strand cDNAs were synthesized from total RNA with SuperScript II reverse transcriptase (Invitrogen). The SPR2 and SP2L cDNA were amplified by PCR using SPR2- and SP2L-specific primers; 5′-TGGTGCAGTCCCTCGTCCAACC-3′ and 5′-GTTCCATTGGAACTCCAAACGT-3′ for SPR2; 5′-CTGTGGAACATCAAGG-AATAGG-3′ and 5′-ACTCCAACGGTATTCCCATAAA-3′ for SP2L. Simultaneous detection of both SPR2 and SP2L cDNAs was performed using common primers that recognized sequences conserved in SPR2 and SP2L cDNAs; 5′-GCA[C/G][T/C]T[G/A]GAGAGACAACAAAC-3′ and 5′-GG[A/C]GC[T/A][A/G]G-ACCTTCCCAGTC-3′. Actin 8 was used as a control (Shoji et al., 2004).

In vivo analysis of microtubule dynamics

Four-day-old seedlings expressing GFP-TUB6 or GFP-EB1b were used for the analysis of microtubule dynamics in the epidermal cells of upper hypocotyl and lower petiole, and in cotyledon guard cells. We used a DMRE microscope (Leica) equipped with a CSU10 scanning head (Yokogawa, Tokyo, Japan) and ORCA-ERCCD camera (Hamamatsu Photonics, Shizuoka, Japan). Images were taken every 2 or 4 seconds during the course of 5 or 6 minutes. The length of microtubules and the movement of EB1 were measured using Scion Image (http://www.scioncorp.com/) with previously developed plugins (Nakamura et al., 2004). We defined the pause state as the period when no significant change in microtubule length (<1 μm/minute) occurs for more than 4 seconds. The track of GFP-EB1 and kimographs were drawn by ImageJ version 1.37 (http://rsb.info.nih.gov/ij) with previously developed plugins (Ishida et al., 2007).

Images of cortical microtubule arrays in epidermal cells were taken from an upper region of hypocotyls and the basal part of petioles of GFP-TUB6 seedlings by confocal laser-scanning microscopy. The microtubule angles were determined with respect to the cell's longitudinal axis by ImageJ.

Co-sedimentation assay of microtubules

Tubulin was isolated from porcine brain by two cycles of polymerization and depolymerization and was purified by Resource Q column chromatography (GE Healthcare) as described previously (Itoh et al., 1997). Microtubule co-sedimentation assays were done basically as described previously (Shoji et al., 2004). Taxol-stabilized microtubules and recombinant SPR2/SP2L fragments with various tags were incubated at 37°C for 15 minutes, the mixtures were centrifuged at 100,000 ***g*** for 10 minutes. Proteins in the supernatant and the pellet were separated by 15% (Ne, Nf), 12.5% (Na, Nb, Nc and Nd), and 10% (others) SDS-PAGE and then stained with Coomassie Brilliant Blue or detected by immunoblotting using 6×His monoclonal antibody (BD Biosciences). Bovine serum albumin (Pierce) was used as a control.

In vitro analysis of microtubule dynamics

Microtubule dynamics were observed in vitro by dark-field microscopy (Nikon ECLIPSE E600 with a Nikon dark-field condenser), according to Nakao et al. (Nakao et al., 2004). In vitro microtubule dynamics were observed by dark-field microscopy. Tubulin at a concentration of 30 μM was polymerized in PEM buffer containing 1 mM GTP. After incubation for 5 minutes at 37°C, an equal volume of TF-SPR2, TF-SP2L or TF was added to make a final concentration of 15 μM for tubulin and 0.2 or 0.4 μM for recombinant proteins. To measure changes in microtubule length, we used the video images incorporated into a Power Mac G4 with the aid of an image capture board (LG3; Scion) in real time using NIH Image. The faster growing end of microtubules is referred to as the plus end while the slower growing end is defined as the minus end. We defined a pause as a growth period in which no significant microtubule change in length (<0.15 μm/minute) occurs for more than 30 seconds.

We thank Patricia Zambryski for pBS-2xrsGFP, Tsuyoshi Nakagawa for pGWB1, and Mika Yoshimura for technical assistance. The SALK Institute Genomic Analysis Laboratory and the Arabidopsis Biological Resource Center is acknowledged for providing the T-DNA knockout alleles and the genomic clones. The work was partly supported by a grant (no. 17027018) and Global COE Program in NAIST (Frontier Biosciences: strategies for survival and adaptation in a changing global environment); MEXT; Japan; by Ground-based Research for Space Utilization promoted by Japan Space Forum; and by NOVARTIS Foundation (Japan) for the Promotion of Science, to T.H.

References

Abe, T. and Hashimoto, T. (2005). Altered microtubule dynamics by expression of modified α-tubulin protein causes right-handed helical growth in transgenic *Arabidopsis* plants. *Plant J.* **43**: 191-204.

Akhmanova, A. and Steinmetz, M. O. (2008). Tracking the ends: a dynamic protein network controls the fate of microtubule tips. *Nat. Rev. Mol. Cell Biol.* **9**, 309-322.

Al-Bassam, J., Larsen, N. A., Hyman, A. A. and Harrison, S. C. (2007). Crystal structure of a TOG domain: conserved features of XMAP215/Dis1-family TOG domains and implications for tubulin binding. *Structure* **15**, 355-362.

Ambrose, J. C., Shoji, T., Kotzer, A. M., Pighin, J. A. and Wasteneys, G. O. (2007). The Arabidopsis CLASP gene encodes a microtubule-associated protein involved in cell expansion and division. *Plant Cell* **19**, 2763-2775.

Arnal, I., Karsenti, E. and Hyman, A. A. (2000). Structural transitions at microtubule ends correlate with their dynamic properties in *Xenopus* egg extracts. *J. Cell Biol.* **149**, 767-774.

Bieling, P., Laan, L., Schek, H., Munteanu, E. L., Sandblad, L., Dogterom, M., Brunner, D. and Surrey, T. (2007). Reconstitution of a microtubule plus-end tracking system *in vitro*. *Nature* **450**, 1100-1105.

Bisgrove, S. R., Hable, W. E. and Kropf, D. L. (2004). +TIPs and microtubule regulation. The beginning of the plus end in plants. *Plant Physiol.* **136**, 3855-3863.

Brittle, A. and Ohkura, H. (2005). Mini spindles, the XMAP215 homologue, suppresses pausing of interphase microtubules in *Drosophila*. *EMBO J.* **24**, 1387-1396.
Brouhard, G. J., Stear, J. H., Noetzel, T. L., Al-Bassam, J., Kinoshita, K., Harrison, S. C., Howard, J. and Hyman, A. A. (2008). XMAP215 is a processive microtubule polymerase. *Cell* **132**, 79-88.
Buschmann, H., Fabri, C. O., Hauptmann, M., Hutzler, P., Laux, T., Lloyd, C. W. and Schäffner, A. R. (2004). Helical growth of the *Arabidopsis* mutant *tortifolia1* reveals a plant-specific microtubule-associated protein. *Curr. Biol.* **14**, 1515-1521.
Chan, J., Calder, G., Fox, S. and Lloyd, C. (2007). Cortical microtubule arrays undergo rotary movements in *Arabidopsis* hypocotyl epidermal cells. *Nat. Cell Biol.* **9**, 171-175.
Clough, S. J. and Bent, A. F. (1998). Floral dip: a simplified method for Agrobacterium mediated transformation of Arabidopsis thaliana. *Plant J.* **16**, 735-743.
Crawford, K. M. and Zambryski, P. C. (2000). Subcellular localization determines the availability of non-targeted proteins to plasmodesmatal transport. *Curr. Biol.* **10**, 1032-1040.
Desai, A. and Mitchison, T. J. (1997). Microtubule polymerization dynamics. *Annu. Rev. Cell Dev. Biol.* **13**, 83-117.
Dixit, R. and Cyr, R. (2004). Encounters between dynamic cortical microtubules promote ordering of the cortical array through angle-dependent modifications of microtubule behavior. *Plant Cell* **16**, 3274-3284.
Furutani, I., Watanabe, Y., Prieto, R., Masukawa, M., Suzuki, K., Naoi, K., Thitamadee, S., Shikanai, T. and Hashimoto, T. (2000). The *SPIRAL* genes are required for directional control of cell elongation in *Arabidopsis thaliana*. *Development* **127**, 4443-4453.
Gard, D. L. and Kirschner, M. W. (1987). Microtubule assembly in cytoplasmic extracts of *Xenopus* oocytes and eggs. *J. Cell Biol.* **105**, 2191-2201.
Gardiner, J. and Marc, J. (2003). Putative microtubule-associated proteins from the Arabidopsis genome. *Protoplasma* **222**, 61-74.
Grego, S., Cantillana, V. and Saimon, E. D. (2001). Microtubule treadmilling in vitro investigated by fluorescence speckle and confocal microscopy. *Biophys. J.* **81**, 66-78.
Hamada, T., Igarashi, H., Itoh, T. J., Shimmen, T. and Sonobe, S. (2004). Characterization of a 200 kDa microtubule-associated protein of tobacco BY-2 cells, a member of the XMAP216/MOR1 family. *Plant Cell Physiol.* **45**, 1233-1242.
Ishida, T., Kaneko, Y., Iwano, M. and Hashimoto, T. (2007). Helical microtubule arrays in a collection of twisting tubulin mutants of *Arabidopsis thaliana*. *Proc. Natl. Acad. Sci. USA* **104**, 8544-8549.
Itoh, T. J., Hisanaga, S., Hosoi, T., Kishimoto, T. and Hotani, H. (1997). Phosphorylation states of microtubule-associated protein 2 (MAP2) determine the regulatory role of MAP2 in microtubule dynamics. *Biochemistry* **36**, 12574-12582.
Kawamura, E., Himmelspach, R., Rashbrooke, M. C., Whittington, A. T., Gale, K. R., Collings, D. A. and Wasteneys, G. O. (2006). MICROTUBULE ORGANIZATION 1 regulates structure and function of microtubule arrays during mitosis and cytokinesis in the Arabidopsis root. *Plant Physiol.* **140**, 102-114.
Kirik, V., Herrmann, U., Parupalli, C., Sedbrook, J. C., Ehrhardt, D. W. and Hülskamp, M. (2007). CLASP localizes in two discrete patterns on cortical microtubules and is required for cell morphogenesis and cell division in Arabidopsis. *J. Cell Sci.* **120**, 4416-4425.
Moore, R. C., Zhang, M., Cassimeris, L. and Cyr, R. J. (1997). In vitro assembled plant microtubules exhibit a high state of dynamic instability. *Cell Motil. Cytoskeleton* **38**, 278-286.
Nakagawa, T., Kurose, T., Hino, T., Tanaka, K., Kawamukai, M., Niwa, Y., Toyooka, K., Matsuoka, K., Jinbo, T. and Kimura, T. (2007). Development of series of gateway binary vectors, pGWBs, for realizing efficient construction of fusion genes for plant transformation. *J. Biosci. Bioeng*. **104**, 34-41.
Nakajima, K., Furutani, I., Tachimoto, H., Matsubara, K. and Hashimoto, T. (2004). SPIRAL1 encodes a plant-specific microtubule-localized protein required for directional control of rapidly expanding *Arabidopsis* cells. *Plant Cell* **16**, 1178-1190.
Nakamura, M., Naoi, K., Shoji, T. and Hashimoto, T. (2004). Low concentrations of propyzamide and oryzalin alter microtubule dynamics in *Arabidopsis* epidermal cells. *Plant Cell Physiol.* **45**, 1330-1334.
Nakao, C., Itoh, T. J., Hotani, H. and Mori, N. (2004). Modulation of the stathmin-like microtubule destabilizing activity of RB3, a neuron-specific member of the SCG10 family, by its N-terminal domain. *J. Biol. Chem.* **279**, 23014-23021.
Rusan, N. M., Fagerstrom, C. J., Yvon, A. M. and Wadsworth, P. (2001). Cell cycle-dependent changes in microtubule dynamics in living cells expressing green fluorescent protein-α tubulin. *Mol. Biol. Cell* **12**, 971-980.
Schek, H. T., III, Gardner, M. K., Cheng, J., Odde, D. J. and Hunt, A. J. (2007). Microtubule assembly dynamics at the nanoscale. *Curr. Biol.* **17**, 1445-1455.
Sedbrook, J. C., Ehrhardt, D. W., Fisher, S. E., Scheible, W. R. and Somerville, C. R. (2004). The Arabidopsis *sku6/spiral1* gene encodes a plus end-localized microtubule-interacting protein involved in directional cell expansion. *Plant Cell* **16**, 1506-1520.
Shaw, S. L., Kamyar, R. and Ehrhardt, D. W. (2003). Sustained microtubule treadmilling in *Arabidopsis* cortical arrays. *Science* **300**, 1715-1718.
Shirasu-Hiza, M., Coughlin, P. and Mitchison, T. (2003). Identification of XMAP215 as a microtubule-destabilizing factor in *Xenopus* egg extract by biochemical purification. *J. Cell Biol.* **161**, 349-358.
Shoji, T., Narita, N. N., Hayashi, K., Asada, J., Hamada, T., Sonobe, S., Nakajima, K. and Hashimoto, T. (2004). Plant-specific microtubule-associated protein SPIRAL2 is required for anisotropic growth in Arabidopsis. *Plant Physiol.* **136**, 3933-3944.
Slep, K. C. and Vale, R. D. (2007). Structural basis of microtubule plus end tracking by XMAP215, CLIP-170, and EB1. *Mol. Cell* **27**, 976-991.
Tirnauer, J. S., Grego, S., Salmon, E. D. and Mitchison, T. J. (2002). EB1-microtubule interactions in *Xenopus* egg extracts: role of EB1 in microtubule stabilization and mechanisms of targeting to microtubules. *Mol. Biol. Cell* **13**, 3614-3626.
Toso, R. J., Jordan, M. A., Farrell, K. W., Matsumoto, B. and Wilson, L. (1993). Kinetic stabilization of microtubule dynamic instability in vitro by vinblastine. *Biochemistry* **32**, 1285-1293.
Tran, P. T., Walker, R. A. and Salmon, E. D. (1997). A metastable intermediate state of microtubule dynamic instability that differs significantly between plus and minus ends. *J. Cell Biol.* **138**, 105-117.
Twell, D., Park, S. K., Hawkins, T. J., Schubert, D., Schmidt, R., Smertenko, A. and Hussey, P. J. (2002). MOR1/GEM1 has an essential role in the plant-specific cytokinetic phragmoplast. *Nat. Cell Biol.* **4**, 711-714.
Vos, J. W., Dogterom, M. and Emons, A. M. (2004). Microtubules become more dynamic but not shorter during preprophase band formation: a possible "search-and-capture" mechanism for microtubule translocation. *Cell Motil. Cytoskeleton* **57**, 246-258.
Zimmermann, P., Hirsch-Hoffmann, M., Henning, L. and Gruissem, W. (2004). GENEVESTIGATOR: *Arabidopsis thaliana* microarray database and analysis toolbox. *Plant Physiol.* **136**, 2621-2632.